Time-dependent inversion estimates of global biomass-burning CO emissions using Measurement of Pollution in the Troposphere (MOPITT) measurements

Avelino F. Arellano Jr.,[1,2] Prasad S. Kasibhatla,[1] Louis Giglio,[3] Guido R. van der Werf,[4] James T. Randerson,[5] and G. James Collatz[6]

[1] We present an inverse-modeling analysis of CO emissions using column CO retrievals from the Measurement of Pollution in the Troposphere (MOPITT) instrument and a global chemical transport model (GEOS-CHEM). We first focus on the information content of MOPITT CO column retrievals in terms of constraining CO emissions associated with biomass burning and fossil fuel/biofuel use. Our analysis shows that seasonal variation of biomass-burning CO emissions in Africa, South America, and Southeast Asia can be characterized using monthly mean MOPITT CO columns. For the fossil fuel/biofuel source category the derived monthly mean emission estimates are noisy even when the error statistics are accurately known, precluding a characterization of seasonal variations of regional CO emissions for this source category. The derived estimate of CO emissions from biomass burning in southern Africa during the June–July 2000 period is significantly higher than the prior estimate (prior, 34 Tg; posterior, 13 Tg). We also estimate that emissions are higher relative to the prior estimate in northern Africa during December 2000 to January 2001 and lower relative to the prior estimate in Central America and Oceania/Indonesia during April–May and September–October 2000, respectively. While these adjustments provide better agreement of the model with MOPITT CO column fields and with independent measurements of surface CO from National Oceanic and Atmospheric Administration Climate Monitoring and Diagnostics Laboratory at background sites in the Northern Hemisphere, some systematic differences between modeled and measured CO fields persist, including model overestimation of background surface CO in the Southern Hemisphere. Characterizing and accounting for underlying biases in the measurement model system are needed to improve the robustness of the top-down estimates.

1. Introduction

[2] In recent years, there has been an increasing emphasis on the use of statistical inverse-modeling analysis techniques to characterize the temporal and spatial variability of atmospheric trace gas sources and sinks. Most of the atmospheric tracer inverse-modeling applications have fo-

cused on quantifying atmospheric CO_2 sources and sinks [e.g., *Fan et al.*, 1998; *Bousquet et al.*, 1999; *Kaminski et al.*, 1999; *Law and Rayner*, 1999; *Bousquet et al.*, 2000; *Peylin et al.*, 2002; *Gurney et al.*, 2002, 2003, 2004; *Rödenbeck et al.*, 2003; *Suntharalingam et al.*, 2003], spurred by the availability of multiyear CO_2 measurements from a global network of surface sites. More recently, formal inverse model techniques have also been applied to characterize the tropospheric budgets of reactive gases such as carbon monoxide [e.g., *Bergamaschi et al.*, 2000; *Kasibhatla et al.*, 2002; *Pétron et al.*, 2002; *Müller and Stavrakou*, 2005] and methane [e.g., *Hein et al.*, 1997; *Houweling et al.*, 1999; *Butler et al.*, 2004; *Mikaloff Fletcher et al.*, 2004a, 2004b]. These studies have yielded valuable insights into the uncertainties associated with our understanding of anthropogenic impacts on the atmospheric budgets of these reactive trace gases. In addition, analysis of spatiotemporal variations in atmospheric concentrations of gases such as CO can yield insights into the factors that

---

[1]Nicholas School of the Environment and Earth Sciences, Duke University, Durham, North Carolina, USA.

[2]Now at Atmospheric Chemistry Division, National Center for Atmospheric Research, Boulder, Colorado, USA.

[3]Science Systems and Applications, Inc., Lanham, Maryland, USA.

[4]Faculty of Earth and Life Sciences, Vrije Universiteit Amsterdam, Amsterdam, Netherlands.

[5]Department of Earth System Science, University of California, Irvine, Irvine, California, USA.

[6]NASA Goddard Space Flight Center, Greenbelt, Maryland, USA.

control the variability of atmospheric CO_2 and CH_4 [e.g., *Langenfelds et al.*, 2002; *van der Werf et al.*, 2004; *Suntharalingam et al.*, 2004].

[3] In this study, we explore the extent to which CO measurements from the MOPITT instrument on NASA's Terra satellite can be used in an inverse-modeling framework to constrain the anthropogenic CO budget. Our study builds on several recent inverse-modeling studies focused on quantifying CO sources. Several of these studies have made use of CO measurements from a globally distributed network of surface monitoring sites [e.g., *Bergamaschi et al.*, 2000; *Kasibhatla et al.*, 2002; *Pétron et al.*, 2002] to quantify the global CO budget. Other inverse-modeling studies have focused on a more detailed regional analysis of CO sources using airborne CO measurements [e.g., *Palmer et al.*, 2003; *Heald et al.*, 2004; *Wang et al.*, 2004]. More recently, several inverse-modeling studies using newly available remote sensing CO measurements have been published. In the first application of its kind, *Arellano et al.* [2004] used CO retrievals from the MOPITT instrument [*Deeter et al.*, 2003] on NASA's EOS Terra satellite in a time-independent Bayesian synthesis inversion to derive geographically disaggregated, annual mean estimates of CO emissions on a global scale from fossil fuel/biofuel use and biomass burning. *Pétron et al.* [2004] performed a similar analysis, but estimated emissions at a monthly rather than annual timescale. The MOPITT CO measurements have also been used in other studies focused on elucidating the CO budget for specific regions [*Allen et al.*, 2004; *Heald et al.*, 2004; *Pfister et al.*, 2004; *Liu et al.*, 2005], assessing the effect of burning on atmospheric chemical composition [*Edwards et al.*, 2003; *Bremer et al.*, 2004; *Edwards et al.*, 2004], and characterizing pollution transport events [*Heald et al.*, 2003; *Lamarque et al.*, 2003; *Gros et al.*, 2004; *Kar et al.*, 2004; *Choi et al.*, 2005; *Li et al.*, 2005].

[4] In the inverse-modeling study presented here, we extend our previous time-independent analysis [*Arellano et al.*, 2004] to estimate the seasonal variation of anthropogenic CO emission, with a particular focus on emissions from biomass burning. In this respect, our study is most closely related to the inverse-modeling study by *Pétron et al.* [2004]. There are, however, some significant differences between our study and the *Pétron et al.* [2004] study. Most importantly, we explore the information content of the MOPITT measurements using a pseudo data analysis approach and provide insights into the extent to which temporal CO source variations can be deduced. In addition, we perform a detailed comparison of independent surface CO measurements from a global monitoring network to evaluate the robustness of the inverse source estimates.

2. Bayesian Synthesis Inversion

[5] The source estimation procedure is based on the statistical linear model

$$\mathbf{y} = \mathbf{Kx} + \boldsymbol{\varepsilon}, \qquad (1)$$

where the measured CO concentration vector $\mathbf{y}$ can be expressed as a linear combination of modeled CO concentrations from individual source categories ($\mathbf{Kx}$) plus

an error vector $\boldsymbol{\varepsilon}$ associated with both the modeled and observed concentrations. The elements of the source vector $\mathbf{x}$ (referred to as basis functions) represent the individual source categories to be estimated. The Jacobian matrix $\mathbf{K}$, which maps the sources to the concentrations, is a matrix of response functions calculated using an atmospheric chemical transport model (CTM). The error vector $\boldsymbol{\varepsilon}$ (referred to as the observation error vector) represents the effects of measurement as well as CTM errors. The inverse problem is to find a vector of source strengths $\hat{\mathbf{x}}$ that produces the best match of the modeled CO concentrations $\mathbf{K}\hat{\mathbf{x}}$ with the measurements, taking into account measurement and CTM errors in a statistical sense and subject to certain a priori constraints on $\mathbf{x}$. Under the specific assumptions that errors and prior knowledge of $\mathbf{x}$ can be described in terms of the multivariate normal distributions $\boldsymbol{\varepsilon} \sim \text{MVN}(\mathbf{0}, \mathbf{S_e})$ and $\mathbf{x_{prior}} \sim \text{MVN}(\mathbf{x_a}, \mathbf{S_a})$, respectively, the maximum a posteriori (MAP) estimate of $\mathbf{x}$ is given by [e.g., *Rodgers*, 2000]

$$\hat{\mathbf{x}} = \mathbf{x_a} + \mathbf{G}(\mathbf{y} - \mathbf{Kx_a}), \qquad (2)$$

with

$$\mathbf{G} = (\mathbf{K}^T \mathbf{S_e}^{-1} \mathbf{K} + \mathbf{S_a}^{-1})^{-1} \mathbf{K}^T \mathbf{S_e}^{-1}, \qquad (3)$$

where $\mathbf{x_a}$ is the a priori source estimate vector, $\mathbf{S_a}$ is the corresponding prior error covariance matrix, and $\mathbf{S_e}$ is the observation error covariance matrix. The a posteriori error covariance matrix $\hat{\mathbf{S}}$ corresponding to the MAP estimate $\hat{\mathbf{x}}$ is given by

$$\hat{\mathbf{S}} = (\mathbf{K}^T \mathbf{S_e}^{-1} \mathbf{K} + \mathbf{S_a}^{-1})^{-1}. \qquad (4)$$

2.1. Prior Sources

[6] We consider three CO source sectors in the inverse analysis study. These are fossil fuel/biofuel combustion (FFBF), biomass burning (BIOM) and chemical oxidation of biogenic nonmethane hydrocarbon (NMHC) emissions (BIOG). CO from methane oxidation is presubtracted in the inversion since this source contributes a relatively uniform background CO mixing ratio field in the troposphere. The a priori annual-averaged FFBF source is specified as in our previous studies [*Kasibhatla et al.*, 2002; *Arellano et al.*, 2004] and is based on the EDGARv2/GEIA inventory [*Olivier et al.*, 1996]. This source, which is representative of the 1990s, includes CO emissions from industrial processes, power generation, fuel extraction, residential and transport sectors. As in our previous studies, we include in the source category CO chemical production from the oxidation of NMHCs emitted because of fossil fuel/biofuel use.

[7] The biomass-burning CO source is specified as given by *Arellano et al.* [2004] using the global fire emission product from *van der Werf et al.* [2003]. The monthly varying CO emissions are derived by an integrated approach involving satellite observations of fire activity from Tropical Rainfall Measuring Mission−Visible and Infrared Spectrometer (TRMM-VIRS), European Remote Sensing Satellite−Along Track Scanning Radiometer (ERS-ATSR) and Terra MODerate resolution Imaging Spectroradiometer

(Terra-MODIS), the Carnegie-Ames-Stanford Approach (CASA) biogeochemical model, and biome-dependent emission factors [*Andreae and Merlet*, 2001].

[8] The a priori BIOG CO is specified using the standard tagged CO scheme in GEOS-CHEM CTM [*Heald et al.*, 2004] and accounts for CO derived from isoprene, monoterpene, methanol and acetone oxidation. The baseline isoprene emission distribution by land type is taken from *Guenther et al.* [1995], with light and temperature dependencies from *Wang et al.* [1998] and *Guenther et al.* [1995], respectively. CO produced from isoprene oxidation is calculated using NO_x-dependent yields (0.16[NO_x ppm] + 0.12 on a per carbon basis, with a minimum threshold at [NO_x] < 0.5 ppm equal to 0.16 and maximum threshold at [NO_x] > 1.8 ppm equal to 0.42). Production of CO from oxidation of monoterpenes is calculated using monoterpene emissions from *Guenther et al.* [1995] using a CO yield of 0.2 molecule on a per carbon basis [*Hatakeyama et al.*, 1991]. The CO source from methanol oxidation is assumed to be 100 Tg/yr, distributed according to the baseline isoprene emissions pattern. CO from acetone is calculated using a biogenic acetone emission inventory archived from a 1994 GEOS-CHEM CTM simulation [*Jacob et al.*, 2002] and using a CO yield of 0.67 on a per carbon basis. During the April 2000 to March 2001 time period considered here, our a priori FFBF, BIOM, and BIOG sources total 604, 501, and 492 Tg CO, respectively. In section 3, we describe the specific choice of the disaggregated basis functions considered in this study.

2.2. Forward Model

[9] The contribution of each basis function considered (see section 3) in our analysis to the total model CO column for each month (referred as Jacobian or response function) is calculated using the tagged CO scheme of GEOS-CHEM CTM v5.05-03, which is driven by NASA/GMAO assimilated meteorological fields [*Bey et al.*, 2001] (see also http://www-as.harvard.edu/chemistry/trop/geos/). For each source category/region/month considered, the CTM propagates the CO signal resulting from the monthly source pulse forward for an 8-month period. We limit the simulation to an 8-month transport and chemical loss period for computational expediency. This period is sufficient for CO, given its average lifetime of about 2 months.

[10] The chemical loss of CO for each basis function is calculated using prescribed monthly mean OH fields from a full tropospheric chemical simulation for the year 2000 and 2001 [*Fiore et al.*, 2003]. The prescribed OH fields correspond to a global lifetime of methyl chloroform against the tropospheric OH sink of about 6.4 years, consistent with recent estimates by *Prinn et al.* [2001]. The chemical production of CO from methane (CH_4) oxidation, which is presubtracted in the inversion, is calculated in GEOS-CHEM using the prescribed OH fields and prescribed CH_4 concentration fields in different latitude bands (90°−30°S, 1706 ppbv; 30°S to equator, 1716 ppbv; equator to 30°N, 1760 ppbv; 30°−90°N, 1814 ppbv). The updated CH_4 fields are based on annual mean concentration representative of the late 1990s [*Dlugokencky et al.*, 2001]. The CO yield from methane oxidation is assumed to be 0.95 as given by *Kasibhatla et al.* [2002].

2.3. MOPITT CO Columns

[11] The MOPITT instrument on board the NASA TERRA EOS satellite provides tropospheric CO measurements at a spatial resolution of about 22 km × 22 km at nadir, with near-global coverage every 3 days. CO mixing ratios are retrieved at seven different atmospheric levels, nominally corresponding to the surface, 850, 700, 500, 350, 250 and 150 hPa [*Deeter et al.*, 2003]. The Level 2 V3 MOPITT CO retrievals from the first year of MOPITT operation (April 2000 to April 2001) are used in this study. Validation results [*Emmons et al.*, 2004] suggest that MOPITT CO mixing ratios from Phase 1 are high by about 4 ppbv (∼7%) at 700 hPa and about 2 ppbv (∼3%) at 350 hPa, while the MOPITT CO columns have been shown to have an average positive bias of about 5%. It is also worth noting that the estimated standard deviations of the biases are quite large. Comparisons with CO measurements during the TRACE-P campaign also show that the MOPITT column CO retrievals have a positive bias of 6 ± 2% [*Jacob et al.*, 2003]. In this study, the MOPITT CO retrievals are not corrected for a positive bias. It is not presently clear as to how the biases observed in some regions can be extrapolated globally and incorporated as part of the inverse analysis. It should be noted, however, that the biases in the data can possibly influence the magnitude of the source estimates (see section 5).

[12] We employ a procedure for data processing and quality control as in our previous study [*Arellano et al.*, 2004]. Briefly, our analysis is restricted to CO retrievals: (1) containing all seven standard levels between 50°S and 50°N, (2) having <50% of a priori contribution to the retrieval at the 350, 500, and 700 hPa levels, and (3) with retrieved 500 hPa mixing ratio >40 ppbv. This procedure is based on the qualitative data uncertainties described in the MOPITT data quality statement. Since the number of independent pieces of information in each profile retrieval is less than 2 [*Deeter et al.*, 2004; *Heald et al.*, 2004], only CO columns derived from the selected MOPITT CO profile retrievals are used in this analysis. MOPITT CO columns are derived by integrating over all MOPITT vertical levels as given by *Heald et al.* [2004]. The observation vector **y** is constructed by removing the contribution of the a priori CO profile used in the MOPITT retrieval algorithm, as well as the modeled contribution of CO from methane oxidation to the column CO. To enable a direct comparison of the model and measurements, the modeled CO for each basis function is sampled at the horizontal, vertical, and temporal locations corresponding to each of the MOPITT retrievals. MOPITT-equivalent model profiles are then calculated using the appropriate MOPITT averaging kernels, and MOPITT-equivalent model CO columns are then derived for each basis function.

[13] The individual CO columns are averaged over the 4° × 5° horizontal CTM grid and over a daily time period. A monthly average is then calculated for each model grid box. For statistical purposes, monthly averages having less than five daily data points are filtered out in the analysis. For the April 2000 to April 2001 time period considered here, the resulting observation vector **y** consists of 23,980 elements.

2.4. Error Covariances

[14] The observation error covariance matrix (S_e) is constructed as the sum of a model plus representation error
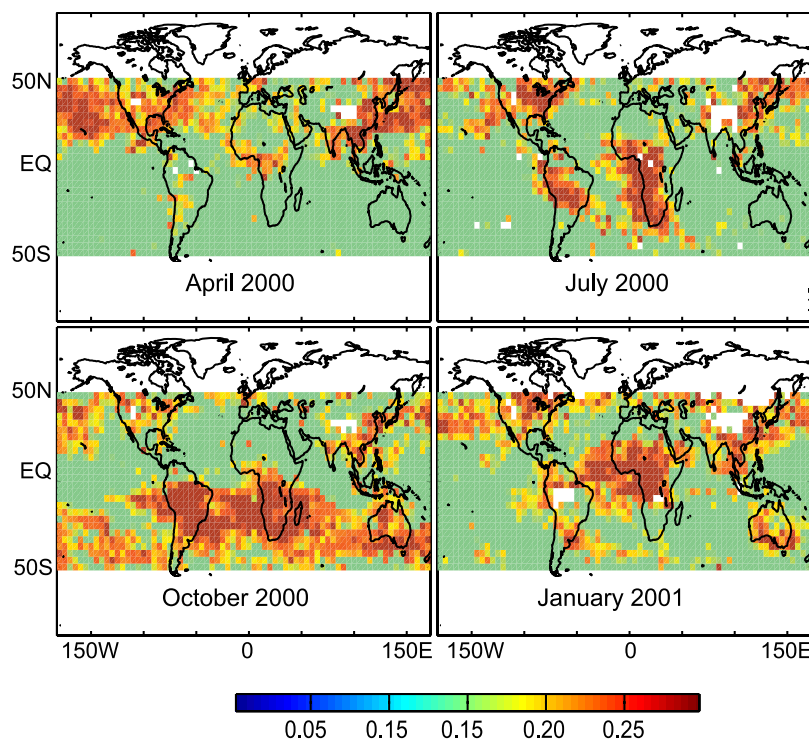
Figure 1. Observation error covariance fields (in 10^{18} molecules cm^{-2}) for selected months. The plotted values represent the diagonal elements of the observation error matrix ($\mathbf{S_e}^{1/2}$).

covariance matrix ($\mathbf{S_m}$) and a retrieval error covariance matrix ($\mathbf{S_r}$). The retrieval error corresponds to the instrument noise as well as errors in the retrieval algorithm, and $\mathbf{S_r}$ is prescribed using the error covariance matrices provided as part of the MOPITT retrievals. The model plus representation error relates to uncertainties in the forward CTM, as well as to errors arising from the assumed source patterns and the mismatch in spatial and temporal scales between the model and the measurements. An analysis by *Jones et al.* [2003] for the February–April 2001 period suggests that characteristic transport model error correlation length scales in the horizontal are of the order of a few hundred kilometers for CO. Given the grid resolution of the CTM used in our analysis, we assume therefore that $\mathbf{S_m}$ is diagonal. Each diagonal element is calculated from the variance of daily mean residuals (MOPITT–a priori model) over the course of the month corresponding to the measurement. This is one of several ad hoc error specifications explored by *Arellano et al.* [2004] and is similar to the approach employed by *Palmer et al.* [2003].

[15] In our analysis, a minimum threshold (0.15 molecule cm^{-2}) is imposed on the individual elements of $\mathbf{S_m}$ for statistical purposes in order to avoid giving too much weight to data points for which there are insufficient number of retrievals to estimate the sample statistics or to regions where the background variability is low. With an a posteriori goodness-of-fit parameter of about 0.5, the resulting observation errors are typically about 8 to 30% of the corresponding monthly mean MOPITT CO columns, with the model plus representation error accounting for the bulk (~98%) of these errors. Maps of the observation errors for selected months are shown in Figure 1. It is readily evident that the observation errors are largest in source and outflow

regions, a feature consistent with transport model error analysis of *Jones et al.* [2003].

[16] The prior source error covariance matrix $\mathbf{S_a}$ is also assumed to be a diagonal matrix. The diagonal elements of the matrix are specified as given by *Arellano et al.* [2004] by assuming that the a priori error for each basis function considered is equal to 50% of the corresponding a priori source estimate.

3. Choice of Basis Functions

[17] An appropriate choice of basis functions is a critical step in any inverse analysis. As a first step in choosing basis functions, we analyze the extent to which the measurements provide information on CO emissions for both the FFBF and the BIOM source categories on a monthly timescale for various geographical regions of interest. Specifically, we define 13 distinct geopolitical regions of interest as shown in Figure 2. We then consider the question as to whether the monthly mean column MOPITT CO column measurements from April 2000 to April 2001 can be used to accurately estimate September 1999 to April 2001 monthly mean emissions from the FFBF and BIOM source categories in each of the 13 regions along with global, annual mean emissions from the BIOG source category. Note that the BIOG prior source does vary seasonally, but its spatial-temporal pattern is fixed in the inversion. We solve for one scalar that adjusts the total strength of this source. Since the short-term interannual variability of FFBF sources is likely small, the assumption of cyclostationarity can be used for FFBF sources. That is, the FFBF emissions for a particular month are considered to be invariant from year to year. Our initial state vector thus comprises 416 elements (i.e.,
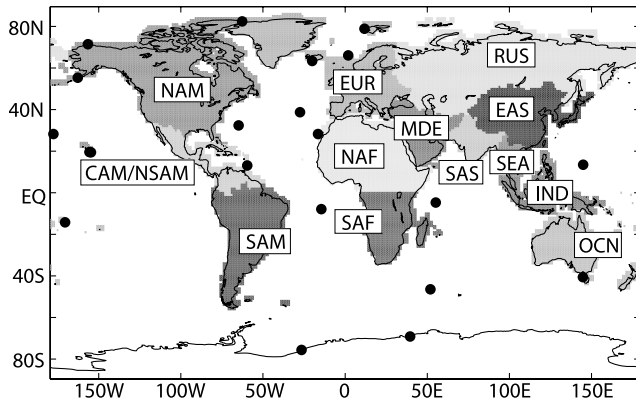
Figure 2. Geographical source regions considered in the inversion analysis. Locations of NOAA CMDL surface measurement sites used for model evaluation are shown with solid circles (see Table 1 for detailed description of sites). NAM, North America; EUR, Europe; RUS, Russia; NAF, northern Africa; CAM/NSAM, Central America/ northern South America; OCN, Oceania; IND, Indonesia; SAS, south Asia; SEA, Southeast Asia; EAS, east Asia; MDE, Middle East; SAF, southern Africa; SAM, South America.

13 regions times 20 months for BIOM, 13 regions times 12 months for FFBF, and one global, annual BIOG).

[18] We focus our analysis on the accuracy of the MAP estimate $\hat{\mathbf{x}}$ of $\mathbf{x}$ during the April 2000 to March 2001 time period. Substituting for $\mathbf{y}$ in equation (2) from equation (1) and rearranging yields the following expression for the error in the MAP estimate $\hat{\mathbf{x}}$:

$$\hat{\mathbf{x}} - \mathbf{x} = (\mathbf{I} - \mathbf{A})(\mathbf{x_a} - \mathbf{x}) + \mathbf{G}\varepsilon, \qquad (5)$$

where the matrix $\mathbf{A} = \mathbf{GK}$ is the averaging kernel associated with the inversion. The first term on the right hand side of equation (5) is termed the smoothing error and the second term the retrieval noise [Rodgers, 2000].

[19] We first consider the ideal case scenario in which the true source magnitudes are assumed to be known and equal to the prior source estimates (i.e., $\mathbf{x} = \mathbf{x_a}$). For this scenario, equation (5) reduces to

$$\hat{\mathbf{x}} - \mathbf{x} = \mathbf{G}\varepsilon. \qquad (6)$$

Since ε is a sample from a multivariate normal distribution with mean $\mathbf{0}$ and error covariance $\mathbf{S_e}$, $\hat{\mathbf{x}}$ is a sample from a multivariate normal with mean $\mathbf{x}$ and error covariance $\mathbf{GS_eG^T}$. Thus an analysis of the matrix $\mathbf{GS_eG^T}$ can shed light on the accuracy of the MAP source estimates for this ideal case.

[20] Given the large number of basis functions considered here, a more convenient way to look at the relevant question as to the accuracy of $\hat{\mathbf{x}}$ for a single realization of ε is to perform a pseudo data analysis using simulated CO fields generated by the CTM with prior source estimates. In Figure 3, we show representative results of such a pseudo data analysis for some of the basis functions considered. The pseudo measurement vector is derived by calculating

the MOPITT-equivalent column CO vector from the model CO concentration fields using the prior source estimates, and perturbing this vector by a random noise vector drawn from a multivariate normal distribution with mean $\mathbf{0}$ and covariance $\mathbf{S_e}$. Also shown in Figure 3 are the 2σ errors of the posterior source estimates as given by the diagonal elements of $\hat{\mathbf{S}}$. It should be noted that $\hat{\mathbf{S}}$ does not depend on the measurements themselves but rather on the inversion setup. Figure 3 shows that even for this ideal case scenario, there are unrealistic short-term oscillations in the posterior FFBF source estimates (compare the blue and black lines). By contrast, the BIOM sources can be accurately retrieved on a monthly timescale. It can also be seen that the a posteriori errors for the monthly FFBF sources are relatively high compared to those for the BIOM sources during months with available constraints from observations. We have conducted an additional pseudo data analysis (not shown here) in which a minimum threshold error of ± 60 Tg CO/yr was employed in specifying the elements of $\mathbf{S_a}$, in order to test the effect of loosening the prior constraints when the prior source estimates are low. We find that this looser constraint affects the accuracy of the retrieved BIOM sources in NAM, EUR, RUS, SAS, and EAS (not shown here) suggesting that these sources are not well resolved by the inverse setup.

[21] To illustrate the effect of the smoothing error, we consider a second case in which the true source vector $\mathbf{x}$ is the same as in the previous case, but the prior source vector $\mathbf{x_a}$ used in the inverse analysis is set equal to $1.5 \mathbf{x}$. The results for this case are also shown in Figure 3. We find that the smoothing error can be significant for some of the FFBF basis functions during certain months (e.g., see the plot for FFBF NAM in Figure 3). We also find that the BIOM source estimates for the major source regions are not degraded when this source of error is considered.

[22] On the basis of these pseudo data analysis tests, we define a reduced set of basis functions that we consider can be adequately resolved using the monthly mean column CO measurements. Specifically, we solve for annual average emissions for the FFBF source category for each of the 13 regions shown in Figure 2, monthly average emissions from eight regions (NAF, SAF, NLA, SLA, NAM, EUR + RUS, OCN + IND, EAS + SAS + SEA + MDE) for the BIOM source category, and the global, annual average BIOG source. Our final set of basis functions thus comprises 174 elements (i.e., eight regions times 20 months for BIOM, 13 regions for FFBF, and one global, annual BIOG). We have repeated the pseudo data analysis tests for this reduced set of basis function and verified that the posterior MAP estimates are accurate for both the FFBF and BIOM source categories (see Figure 4).

[23] An inspection on the elements of $\hat{\mathbf{S}}$ also shows that the posterior errors (2σ) for the major basis functions during months with observations are quite small (6–26% for the annual FFBF sources, and 8–30% for the monthly BIOM sources), indicating the usefulness of MOPITT CO measurements in constraining CO sources. This conclusion seems to be inconsistent with the statement by Pétron et al. [2004] that posterior errors associated with monthly fluxes are not significantly reduced by the MOPITT CO measurements. However, a larger number of monthly fluxes were estimated in the Pétron et al. [2004] study, and it is not
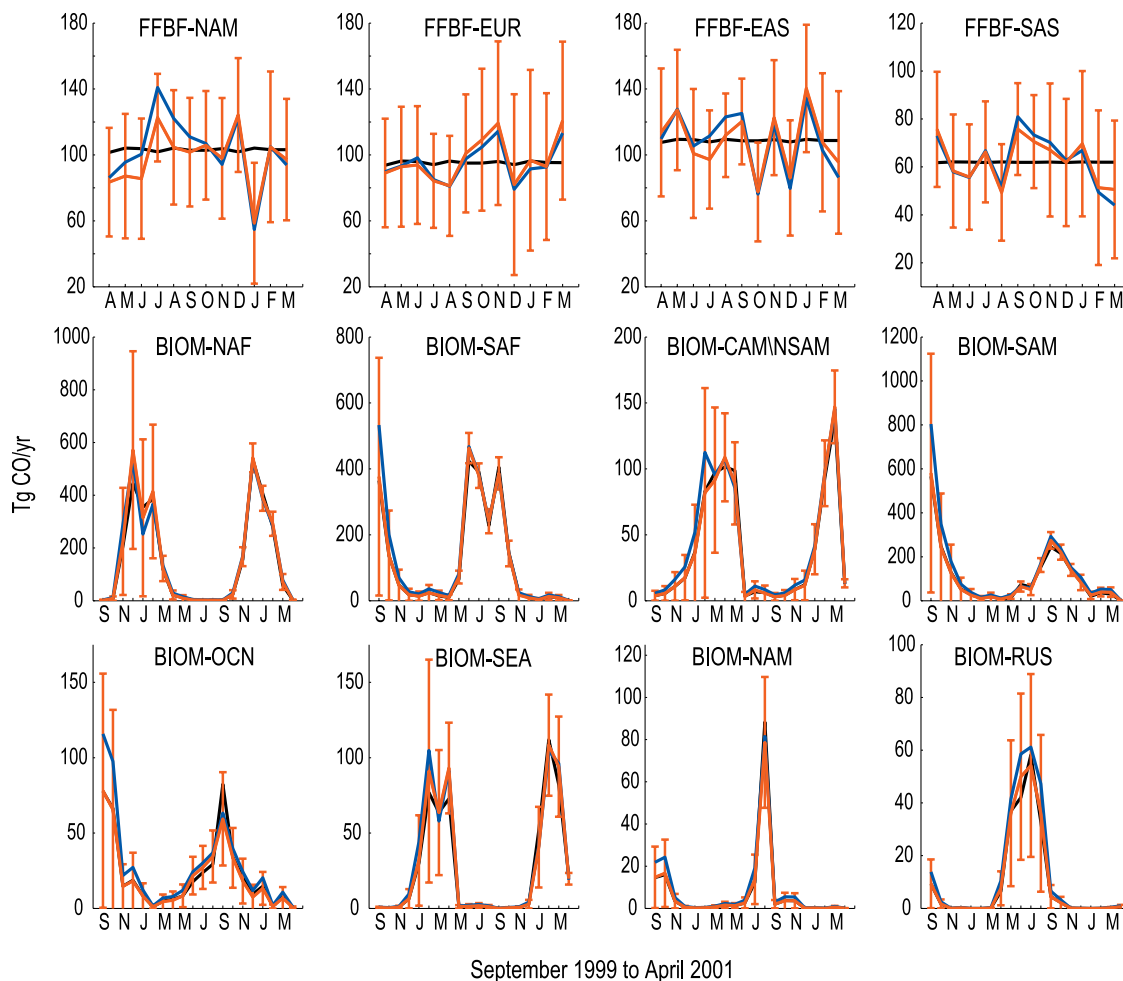
Figure 3. Pseudo data analysis results for initial basis functions. "True" values are in black, and posterior source estimates for cases with and without smoothing error are shown in red and blue, respectively. The posterior error estimates are the same for the two cases. Posterior estimates of the global annual biogenic for the two cases are 483 and 400 Tg CO/yr as compared to the "true" value of 492 Tg CO/yr.

clear whether this is the cause of the apparent difference in the resulting error estimates.

[24] It should be emphasized that our analysis has only focused on the ideal scenario in which the assumed statistical models correctly represent the measurement-modeling system. In reality, however, there will be unaccounted for errors that will result in source estimates that are not accurate. In our analysis of the actual measurements presented in sections 4 and 5 we discuss potential inaccuracies in our source estimates. Nevertheless, the pseudo data analysis presented here sheds some light on the extent to which the measurements provide information on the sources of interest.

4. Inverse Analysis Source Estimates

[25] Time-dependent inversion results for the final basis functions using the MOPITT column measurements are shown in Figure 5. For reference, corresponding values of Figure 5 are made available as auxiliary material (see Table S1)[1]. In sections 4.1 and 4.2 we discuss the

important aspects of our results for the various source categories and regions considered. To facilitate the discussion, measured and modeled CO columns are shown in Figure 6, and the corresponding difference fields are shown in Figure 7. In the rest of this paper, we will refer to the model with the prior and posterior source estimates as the "model prior" and the "model posterior," respectively.

[26] In general, Figures 6 and 7 show that there are some large discrepancies between measured and model prior CO fields. The model prior estimate underestimates CO columns in much of the Northern Hemisphere during spring, with more complex temporal patterns seen in the tropics and the Southern Hemisphere (e.g., model prior estimate overestimates CO during the early part of the burning season and underestimates CO in the latter part of the burning season in both northern and southern Africa). Although the discrepancies are significantly reduced with the inferred posterior sources, some spatial structure persists in the posterior difference fields. This indicates the presence of unaccounted for biases in the inverse analysis. While a full investigation of these biases is beyond the scope of this study, which is based on one particular CTM, we qualify our discussion in sections 4.1 and 4.2 as appropriate to acknowledge this limitation in our analysis.
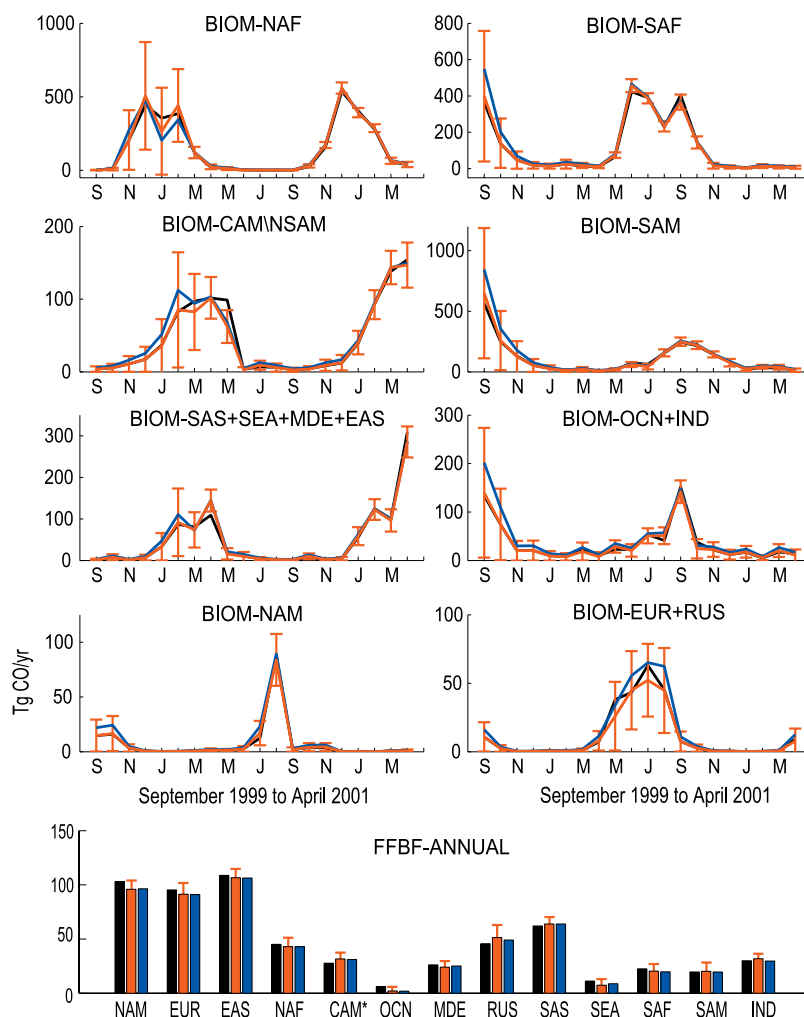

Figure 4. Pseudo data analysis results for final basis functions. "True" values are in black, and posterior source estimates for cases with and without smoothing error are shown in red and blue, respectively. The posterior error estimates are the same for the two cases. Posterior estimates of global annual biogenic for the two cases are 480 and 458 Tg CO/yr as compared to the "true" value of 492 Tg CO/yr.

4.1. Biomass-Burning Sources

[27] A major focus of this study is to examine the seasonal variation of CO emissions due to biomass burning in various regions using the time-dependent inversion approach. While we invert for monthly biomass-burning emissions from September 1999 to April 2001, we focus on the estimates for the April 2000 to March 2001 period, which can be reasonably resolved given the time span (April 2000 to April 2001) of the measurements used in the inverse analysis. Inferences on monthly emissions prior to April 2000 are limited in this respect and must be interpreted as indicative rather than quantitative. Figure 5 shows that in most regions the seasonal variation of the posterior source estimates is roughly consistent with the variation in the prior estimates. This is not surprising because of our assumption that the error in the prior estimate is ±50% of the prior source, leading to posterior estimates close to the prior estimate when the prior estimate is very low. There are, however, some interesting differences in seasonality evident in Figure 5, which we discuss in the succeeding paragraphs.

[28] In northern Africa the posterior source has a more uniform distribution during the 2000/2001 burning season, with a smaller peak in December 2000 but a higher value in March 2001. As seen in Figures 6 and 7, the prior model CO columns within the source and downwind region are overestimated during January 2001 (this is also the case for December which is not shown here) and underestimated during March and April 2001. Similarly, higher emissions relative to the prior estimate in Central America/northern South America and south/Southeast Asia are needed to model the CO columns in the tropics and subtropics of the Northern Hemisphere during spring.

[29] A more pronounced difference between the seasonality of the prior and posterior CO emissions is seen in southern Africa. In addition to the typical peak during the August–September fire season, the prior source also has a strong peak during June and July. In contrast, the posterior source peaks in September and October and monthly emissions in June and July are roughly half the peak value. In a comparative study using MOPITT, SHADOZ ozone and MODIS aerosol measurements, *Bremer et al.* [2004]
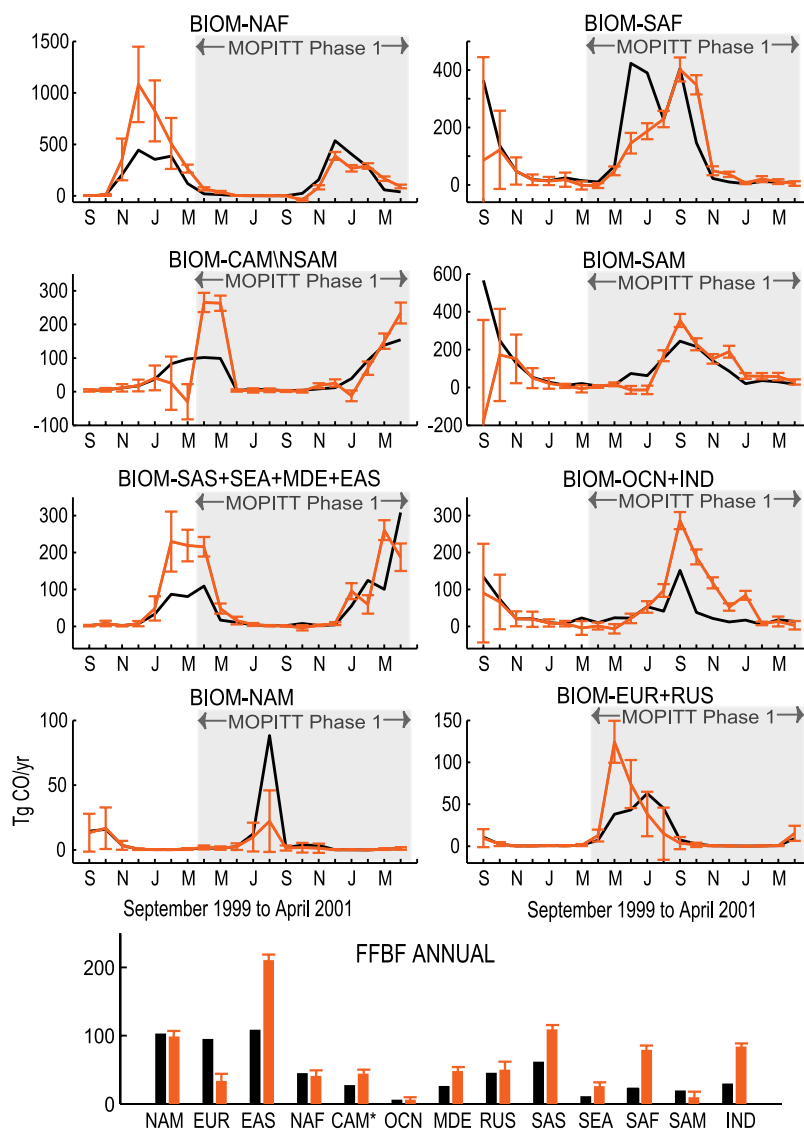
Figure 5. CO source and error estimates (in Tg CO/yr) for the BIOM and FFBF categories from regional sources. A priori sources are indicated with black lines. A posteriori source and 2σ error estimates are shown in red. The posterior estimate from global biogenic source (BIOG) is 394 ± 21 Tg CO/yr compared to the prior source of 492 Tg CO/yr.

showed that the effect of biomass-burning sources in southern Africa is most intense from September to November. They noted that there is a high correlation between CO, ozone and aerosol optical depths at SHADOZ sites near southern Africa suggesting that the September–October peak observed in MOPITT is consistent with other coincident measurements. The adjustment in South America is similar to that in southern Africa during the early part of the burning season, with a lower posterior source relative to the prior source during June and July reflecting the overestimate of CO columns in the prior model in the source region during this period. In the Indonesia/Oceania region, the posterior estimate is significantly higher than the prior estimate for the period between September 2000 and January 2001.

[30] Our analysis suggests that biomass-burning emissions in the Southern Hemisphere are significantly higher

than the prior estimates during the latter part of the burning season, with the reverse being true in the early part of the burning season. Further analysis is required to determine the extent to which shortcomings in the fire model used to derive the prior source estimates can account for this discrepancy. For example, a source of uncertainty that needs to be addressed in the fire model is the apparent difference in spatial patterns of burning detected among different fire products, and the possible changes in emission factors within the burning season and/or within a biome type. It should be noted, however, that even with the higher posterior source estimates, CO column burdens are underestimated over parts of the Southern Ocean and are overestimated over parts of the biomass-burning source regions during the October 2000 to January 2001 time period in the model. It is thus possible that our inverse results are influenced in part by unknown (and unaccounted for in
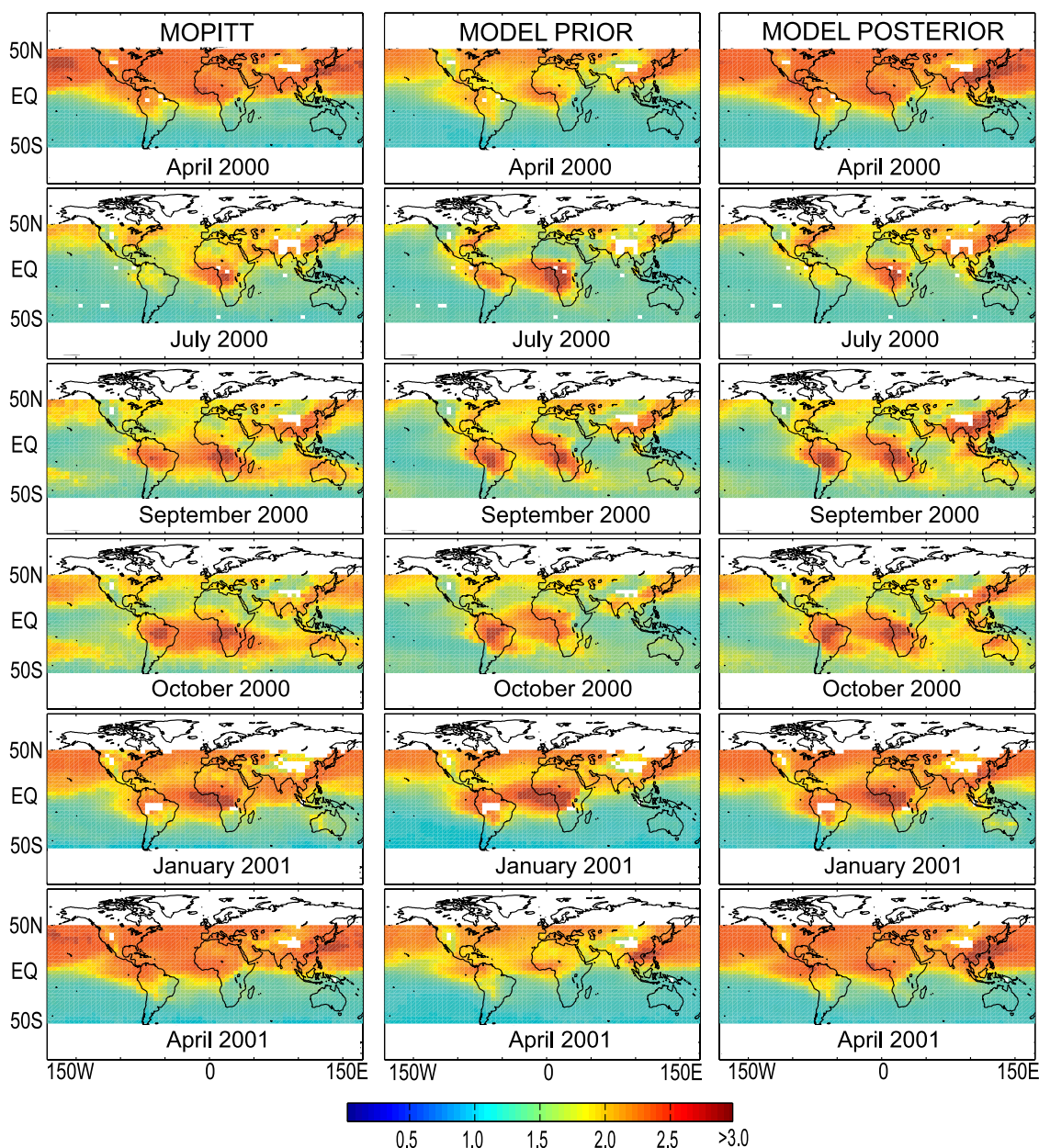
Figure 6. MOPITT, model prior, and model posterior column CO fields for selected months (in 10^{18} molecules cm^{-2}).

the statistical assumptions) model biases in transport and/or aggregation errors due to the large basis function regions considered in our analysis. One source of uncertainty that is difficult to isolate in our analysis is the possible bias in representing vertical transport in the model. This type of error may be particularly relevant to this study since MOPITT is more sensitive to CO in the middle and upper troposphere.

[31] The prior and posterior biomass-burning sources in the boreal regions of the Northern Hemisphere also exhibit important differences. In particular, the posterior source in Europe/Russia clearly peaks 2 months earlier than the prior, and the posterior CO sources are significantly lower than the prior sources in both North America and Europe/Russia during the boreal summer. These changes reflect the under-

estimate of CO columns in the prior model in the middle and high latitudes of the Northern Hemisphere during spring and the underestimate in parts of this region during summer, which results in adjustments to various source categories that affect this region to best match the measurements over the course of the year. It should be noted that the posterior errors for BIOM NAM and BIOM EUR + RUS are relatively large compared to estimates for biomass-burning sources in the tropical region. While it is likely that the source estimates are correlated with the biogenic component in this region, given the similarity in the magnitude of its seasonal variation (see Figure S1), regional source adjustments are constrained in our inversion setup which uses a global, annual biogenic source.
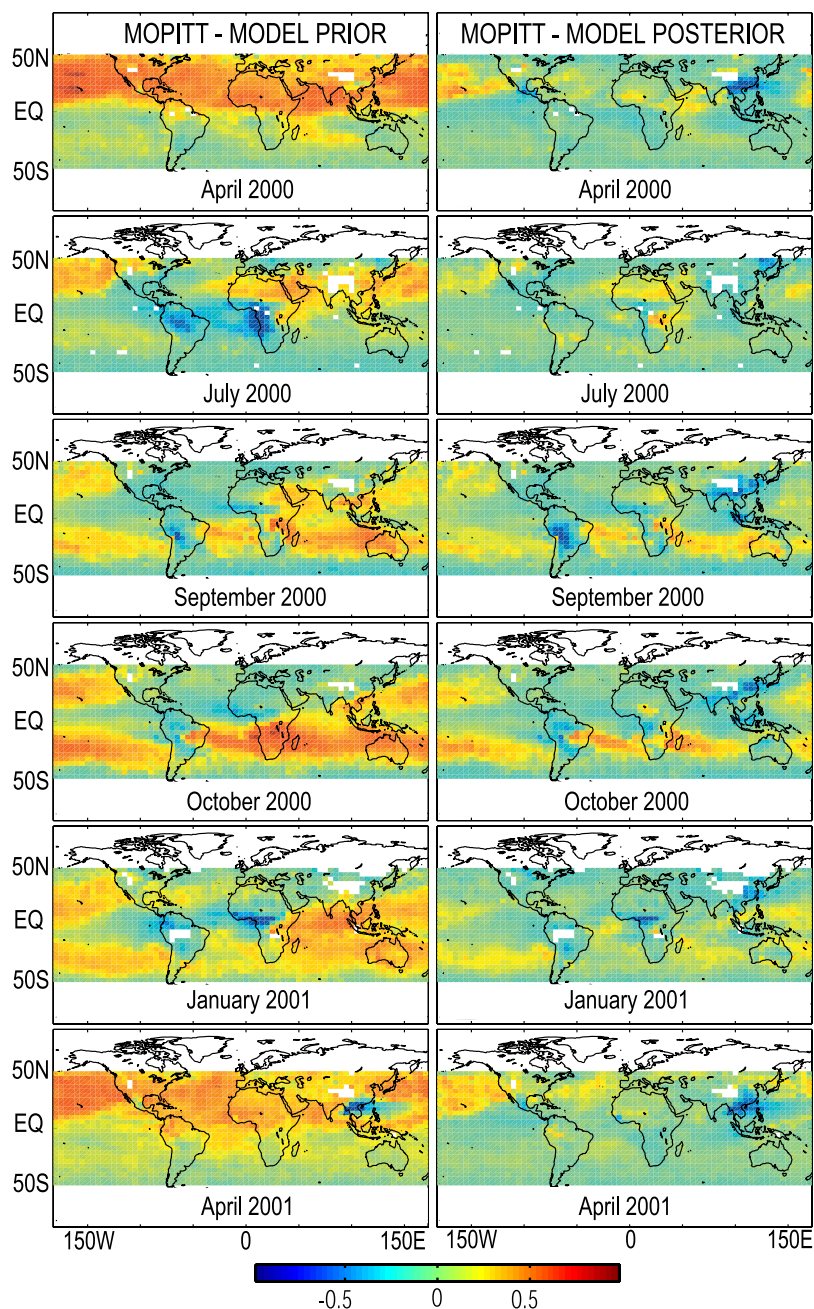
Figure 7. Mismatch between MOPITT and model CO columns for selected months (in 10^{18} molecules cm^{-2}).

[32] Comparisons of the seasonal variations of our source estimates with the estimates derived by *Pétron et al.* [2004] (results obtained from http://acd.ucar.edu/~boris/Science/ EMISSIONS) for the April 2000 to March 2001 time period are shown in Figure 8. Also shown in Figure 8 are the seasonal biomass-burning CO source estimates of *Duncan et al.* [2003], derived using satellite fire count and aerosol index measurements for the September 1999 to December 2000 time period. Figure 8 shows that there is only a limited degree of consistency between the posterior source estimates derived here and the source estimates of *Duncan et al.* [2003] and *Pétron et al.* [2004] in terms of the seasonal variability. For example, our conclusion that the southern

Africa biomass-burning source in June–July 2000 is significantly lower than the prior estimate is consistent with the results of *Duncan et al.* [2003] and *Pétron et al.* [2004]. However, the most notable feature of Figure 8 is the relatively large differences between the various source estimates. For example, our peak estimates are significantly higher in Africa and South America, but match the *Pétron et al.* [2004] peak estimate in Oceania/Indonesia. In the Northern Hemisphere boreal region, our posterior estimate in May 2000 agrees well with the *Duncan et al.* [2003] estimate and is significantly higher than the *Pétron et al.* [2004] estimate. However, the consistency of our estimate with that of *Duncan et al.* [2003] does not hold up in
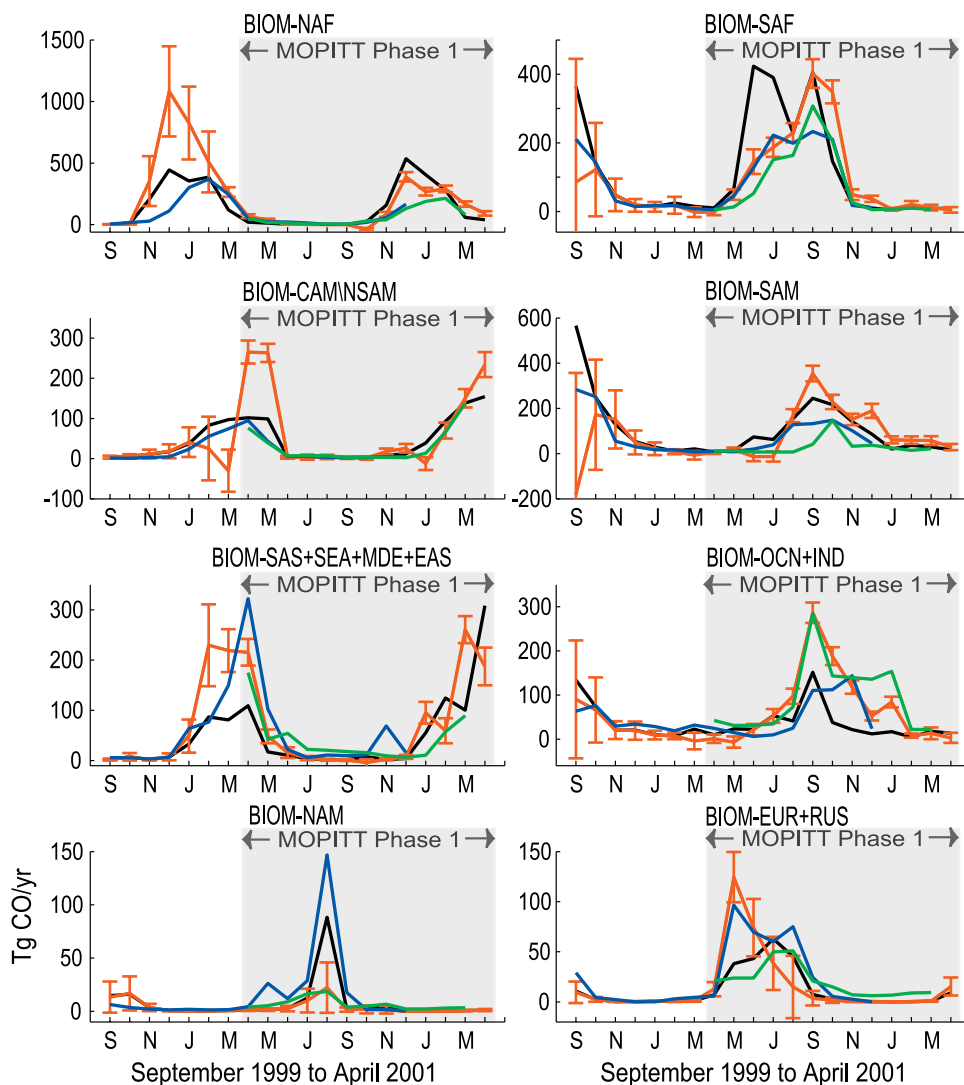
Figure 8. Comparison of prior (black) and posterior (red) biomass-burning CO source estimates with corresponding estimates from *Duncan et al.* [2003] (blue) and *Pétron et al.* [2004] (green).

August 2000, with our estimate being significantly lower and closer to the *Pétron et al.* [2004] estimate. Further research is needed to identify the causes of these differences in biomass-burning emission estimates in order to develop a consistent, spatially and temporally resolved biomass-burning emission data set. We discuss this issue further in the context of inverse modeling in section 7.

4.2. Fossil Fuel/Biofuel and Biogenic Sources

[33] The fossil fuel/biofuel (FFBF) CO posterior annual source estimates shown in Figure 5 are largely consistent with our previous time-independent analysis [*Arellano et al.*, 2004]. It is readily evident that posterior FFBF CO source estimates in Asia are significantly higher than the corresponding prior estimates that are representative of the 1990s. The posterior FFBF CO source estimate for east Asia (211 Tg CO/yr) is consistent with our own previous analysis using surface measurements [*Kasibhatla et al.*, 2002] and is also consistent with other studies focusing on this region [e.g., *Carmichael et al.*, 2003; *Palmer et al.*, 2003; *Allen et al.*, 2004; *Heald et al.*, 2004; *Tan et al.*, 2004; *Wang et al.*,

2004]. The consistency with these latter studies, which have used more up-to-date emission inventories, suggests that our process level understanding of FFBF CO emissions in east Asia is incomplete. This higher posterior estimate relative to the prior estimate reflects the large discrepancy between the prior model and MOPITT CO columns over the North Pacific, particularly during the NH spring season (see Figure 7). The posterior FFBF source estimates for south Asia and Indonesia are also significantly higher than the corresponding prior source estimates, reflecting the underestimates of CO over the Arabian Sea, the Bay of Bengal, and over the tropical eastern Pacific in the prior model (see Figure 7). It is likely that these posterior estimates are biased high given that the posterior modeled CO is biased high relative to the measurements over the Indian subcontinent and in the vicinity of Indonesia during certain times of the year (see Figure 7). There is also a discrepancy between these posterior sources estimates with the inverse-modeling results of *Heald et al.* [2004]. They estimated a total source from fuel combustion as well as biomass burning of about 91 Tg CO and 78 Tg CO for 2001 in

south Asia plus Southeast Asia and Indonesia, respectively. Our combined estimate for these source sectors for the April 2000 to March 2001 time period is 191 Tg CO for south Asia plus Southeast Asia and 114 Tg CO for Indonesia (84 Tg FFBF Indonesia plus 38% of 76 Tg BIOM Oceania plus Indonesia). The cause of these differences in source estimates is not clear and could, in part, be related to differences in the inversion setup (e.g., choice of basis functions used and the data quality control procedures used to screen the measurements) between the two studies. It should also be noted that the *Heald et al.* [2004] study was restricted to an analysis of MOPITT CO measurements over Asia and the adjacent ocean regions during the spring of 2001, while our analysis utilizes measurements over the course of the whole year covering a global domain.

[34] Other differences between prior and posterior source estimates are also evident in Figure 5. While the posterior estimates are consistent with the prior estimates for North America and Russia, the posterior estimate for Europe is significantly lower than the prior. While European CO emissions are reported to be decreasing in recent years, our posterior estimate is most likely too low and is perhaps indicative of an unaccounted for model bias in this region. There is also a large discrepancy of CO between posterior and prior FFBF CO source estimates for Central America and northern South America (44 Tg CO compared to 28 Tg CO) and FFBF southern Africa (79 Tg CO compared to 23 Tg CO). This result is consistent with the large FFBF source estimated by *Arellano et al.* [2004] for their aggregated Rest of the World (ROW) region. Our results for southern Africa support regional observations on increasing energy use in the region. *Lelieveld et al.* [2004] suggested, for example, that the anthropogenic emissions of NO_x, associated with energy use in Africa, has increased substantially and is the likely cause of the observed increase in O_3 trend in the Southern Hemisphere. They noted that the strongest source is located in southern Africa with substantial contribution from western and northern Africa. Increases in biofuel use were also noted in tropical Africa.

[35] Our posterior estimate for the global biogenic source is 394 ± 21 Tg CO/yr, about 20% lower than the prior estimate of 492 Tg CO/yr. This decrease cannot be generally attributed to a specific region or time period since we only solve for a global, annual mean estimate. We also note the posterior biogenic CO source estimate derived here is about a factor of 2 higher than that derived by *Pétron et al.* [2004]. It is not clear, however, whether this difference in the two inverse results is due to differences in the corresponding forward models or due to methodological difference in the inverse analysis. Disaggregating the global biogenic basis function into regional components should provide additional insights into the causes of this difference. More importantly, additional constraints from different measurements (e.g., formaldehyde columns as shown by *Shim et al.* [2005]) and newer bottom-up emission inventories like the MEGAN inventory [*Guenther et al.*, 2006] can provide information that can be incorporated in the inverse analysis. These constraints have the potential to differentiate the atmospheric signals from collocated sources like biomass burning and biogenic emissions. In section 5 we discuss the extent to which surface CO measurements in remote regions of the Southern Hemisphere support the posterior estimate of the biogenic CO source derived here.

5. Comparison of Model Results With Surface Measurements

[36] Figure 9 shows comparisons of monthly mean modeled CO concentrations with surface measurements for selected background sites of National Oceanic and Atmospheric Administration Climate Monitoring and Diagnostics Laboratory (NOAA CMDL) measurement network (see Table 1 for site names and locations). We have restricted our analysis to marine, background sites because assessing the representativeness of the CTM results at sites within or near source regions is difficult given the CTM's coarse grid resolution. Since a variety of sources contribute to the background CO concentrations at each site, the measurements do not provide unambiguous support for source estimates from the inverse analysis. Rather, the comparisons provide an integrated, but nevertheless useful, measure of model performance.

[37] Figure 9 shows that the model posterior reproduces the seasonal cycle at background midlatitude and high-latitude sites (ALT, ZEP, BRW, STM, ICE, CBA, SHM, and AZR) in the Northern Hemisphere. At these sites, the increase due to the higher (relative to the prior source) posterior FFBF-EAS source is more than compensated for by the decrease due to the lower FFBF-EUR source during the fall-winter time period. In addition, the decrease due to the lower posterior biogenic and summertime boreal biomass-burning source contributes to the decreased (relative to the prior) CO during the late summer/early fall time period. The one exception is AZR, where the seasonal cycle is simulated equally well with both the prior and posterior source estimates.

[38] There is also a general improvement in model performance at tropical and subtropical sites in the Northern Hemisphere (BMW, IZO, MID, MLO, KUM, GMI, and RPB). At theses sites, the use of the posterior source estimates leads to better agreement with measured CO during the winter/spring time period. This improvement is due, in part, to the higher posterior FFBF-EAS source, the contribution of which is not fully compensated for at these sites by the lower posterior FFBF-EUR source. In addition, part of the improvement in spring 2000 is due to the higher posterior BIOM sources in North Africa and south/Southeast Asia during this period.

[39] At the tropical and subtropical Southern Hemisphere sites (SMO, ASC, SEY, and EIC), the model prior and posterior CO concentrations are generally comparable. This is a result of compensating changes in the contributions from different sources. There are a couple of interesting exceptions, however. At SEY, the posterior model CO is higher, and in better agreement with the measurements, in January 2001. The higher posterior FFBF source in south Asia contributes significantly to this improvement, during this period when outflow in the lower troposphere from this region to the Indian Ocean is strongest. The different seasonal cycle in the posterior BIOM-SAF source relative to the prior, leads to a corresponding difference in the modeled seasonal cycle of surface CO at ASC. In each case, however, the peak CO concentrations during the
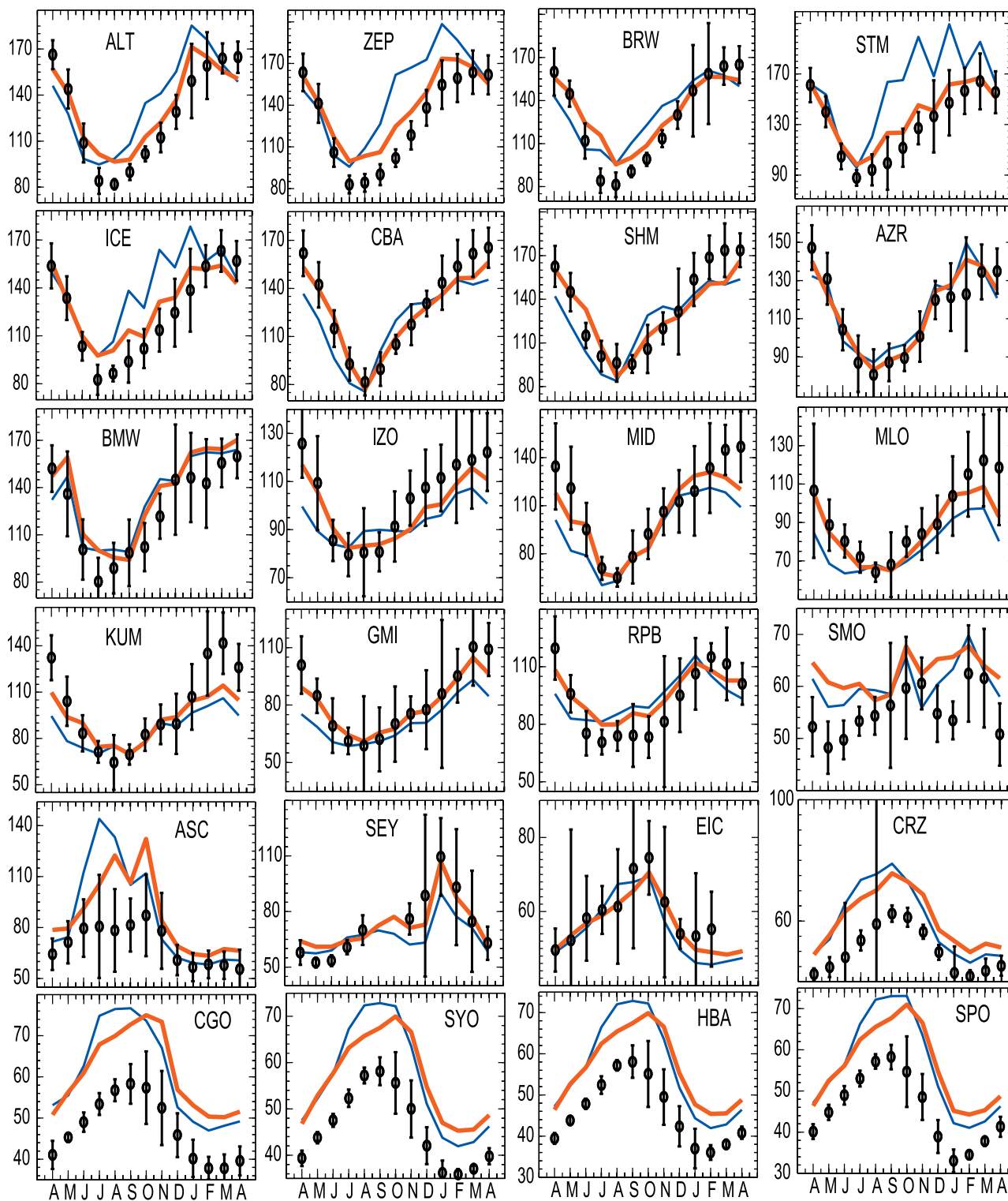
Figure 9. Comparison of modeled surface CO with selected NOAA CMDL station measurements from April 2000 to April 2001. Modeled surface CO (ppbv) for prior and posterior estimates are shown with thin and thick lines, respectively. NOAA CMDL CO values are indicated with circles with 1σ uncertainty (calculated over the 1999–2002 time period) shown as error bars.

Southern Hemisphere biomass-burning season are significantly overestimated in the model. While it is possible that this may be due to a bias in the source estimates for southern Africa, it is also possible that there is an unac-

counted for bias in model transport in this region, where transport of CO from biomass burning over Ascension Island has been shown to take place at a higher vertical level than the observation site. Further investigations (e.g.,

Table 1. NOAA CMDL Measurement Sites Used in the Analysis

Site Code	Sampling Location	Latitude	Longitude
ALT	Alert, Nunavut, Canada	82.45°N	62.52°W
ASC	Ascension Island, United Kingdom	7.92°S	14.42°W
AZR	Terceira Island, Azores, Portugal	38.77°N	27.38°W
BMW	Tudor Hill, Bermuda, United Kingdom	32.27°N	64.88°W
BRW	Barrow, Alaska, United States	71.32°N	156.6°W
CBA	Cold Bay, Alaska, United States	55.2°N	162.72°W
CGO	Cape Grim, Tasmania, Australia	40.68°S	144.68°E
CRZ	Crozet Island, France	46.45°S	51.85°E
EIC	Easter Island, Chile	27.15°S	109.45°W
GMI	Mariana Islands, Guam	13.43°N	144.78°E
HBA	Halley Station, Antarctica, United Kingdom	75.58°S	26.5°W
ICE	Heimaey, Vestmannaeyjar, Iceland	63.25°N	20.15°W
IZO	Tenerife, Canary Islands, Spain	28.3°N	16.48°W
KUM	Cape Kumukahi, Hawaii, United States	19.52°N	154.82°W
MID	Sand Island, Midway, United States	28.22°N	177.37°W
MLO	Mauna Loa, Hawaii, United States	19.53°N	155.58°W
RPB	Ragged Point, Barbados	13.17°N	59.43°W
SEY	Mahe Island, Seychelles	4.67°S	55.17°E
SHM	Shemya Island, Alaska, United States	52.72°N	174.1°E
SMO	Tutuila, American Samoa	14.25°S	170.57°W
SPO	South Pole, Antarctica, United States	89.98°S	24.8°W
STM	Ocean Station M, Norway	66°N	2°E
SYO	Syowa Station, Antarctica, Japan	69°S	39.58°E
ZEP	Ny-Alesund, Svalbard, Norway and Sweden	78.9°N	11.88°E

detailed comparisons with aircraft measurements during SAFARI 2000) are needed to fully elucidate this issue.

[40] At the midlatitude and high-latitude sites in the Southern Hemisphere (CRZ, CGO, SYO, HBA, SPO), the modeled CO concentrations with prior and posterior sources are similar because of compensating changes in CO from different source regions. However, there is a significant discrepancy between the model and the measurements at these sites throughout the year. This year-round discrepancy between the model and measurements is difficult to reconcile in terms of systematic biases in the time-dependent biomass-burning source estimates. An overestimate in the biogenic CO source strength is also unlikely to be the only explanation of this discrepancy. Our lower posterior estimate (394 Tg/yr) relative to the prior estimate (492 Tg/yr) only leads to decrease of 2–3 ppbv in surface CO concentrations at these sites. As we have noted in section 2.3, *Emmons et al.* [2004] have shown that the MOPITT CO column retrievals are biased, on average, by about 5%.

However, limited comparisons with vertical profiles at Rarotonga in the Pacific suggest that the bias at clean sites may be as high as 20–40% (see Figure 6 of *Emmons et al.* [2004]). The extent to which such state-dependent biases in the measurements, as well as other unaccounted for biases in the modeling system, lead to biased source estimates remains to be investigated.

6. Inverse Estimates of Carbon Emissions From Biomass Burning

[41] Having qualified the results of our inverse analysis, we further extend our estimates to include carbon emissions from biomass burning using a similar approach used by *van der Werf et al.* [2004] for biomass-burning anomalies constrained by CMDL CO measurements. Shown in Table 2 are annual estimates of biomass burning derived from our inverse analysis for April 2000 to March 2001 period and the corresponding bulk estimates of carbon emissions de-

Table 2. Estimates of Biomass-Burning CO and Carbon Emissions for the April 2000 to March 2001 Time Period

Region[a]	Prior CO, Tg CO/yr	Posterior CO, Tg CO/yr	Emission Factor,[b] g CO/kg dry matter	Posterior C,[c] Pg C/yr
NAM	10	4 ± 1	83 ± 29	0.02 ± 0.01
EUR + RUS	17	23 ± 3	85 ± 30	0.12 ± 0.06
NAF	125	106 ± 3	71 ± 21	0.67 ± 0.20
CAM/NSAM	43	66 ± 2	81 ± 22	0.37 ± 0.10
OCN + IND	34	76 ± 2	74 ± 23	0.46 ± 0.14
SAS + SEA + EAS + MDE	37	59 ± 2	74 ± 23	0.36 ± 0.11
SAF	144	124 ± 4	69 ± 21	0.81 ± 0.25
SAM	91	105 ± 4	78 ± 22	0.61 ± 0.17
Global	501	563 ± 8	75 ± 23	3.38 ± 1.04

[a]NAM, North America; EUR, Europe; RUS, Russia; NAF, northern Africa; CAM/NSAM, Central America/northern South America; OCN, Oceania; IND, Indonesia; SAS, south Asia; SEA, Southeast Asia; EAS, east Asia; MDE, Middle East; SAF, southern Africa; SAM, South America.

[b]Represents an annual mean and weighted 1σ standard deviation for each region.

[c]Using 45% C per dry matter, carbon source estimates are calculated as posterior CO/emission factor × 0.45. Error estimates include combined uncertainties (in quadrature) from posterior CO and emission factor.

rived using an updated annual mean biome-dependent emission factor for each region of interest. These estimates represent our attempt to link our MOPITT-constrained CO emissions to a biogeochemically important source component of biomass burning. Globally, our estimate of carbon released from biomass burning (3.38 ± 1.04 Pg C/yr) is slightly higher than the mean estimate by *Andreae* [1991] of 3.27 Pg C/yr from fires in savannah, tropical forests, temperate and boreal forests and agricultural waste burning. More importantly, the regional partitioning of carbon emissions show important source contributions of other regions such as Oceania/Indonesia including Southeast Asia (24%) and Central America and northern South America (11%) even for the low-fire period during the year 2000 and early 2001.

7. Summary and Conclusions

[42] In this study, we have extended our previous analysis of MOPITT measurements [*Arellano et al.*, 2004] to explore the extent to which column CO measurements can provide information on anthropogenic CO emissions. The analysis presented here demonstrates that MOPITT CO column measurements, in combination with other satellite-derived fire products, can provide useful information on CO emission from biomass burning on regional and seasonal scales. Under the assumption that errors in the model measurement system are independent and Gaussian, we find that the a posteriori errors (2σ) associated with monthly mean CO source estimates for major sources are about $10-20\%$ of the posterior source estimates. We further find that there are prior and posterior biomass-burning CO source estimates that differ significantly in terms of seasonal variability in some instances. In particular, our analysis of the MOPITT CO measurements suggests that the prior estimates of biomass-burning CO emissions in the Southern Hemisphere are biased high in the early part of the burning season, and biased low in the latter part of the burning season. Our posterior estimates are also higher than the corresponding prior estimates in spring in the Northern Hemisphere tropics and subtropics and in Europe/Russia. The extent to which these differences are due to shortcomings in the fire model used to derive the prior source estimates remains to be investigated.

[43] For the fossil fuel/biofuel CO source category, we find that the monthly mean, posterior regional source estimates are noisy, precluding the quantification of seasonal variations that are expected to be relatively modest. From an annual mean perspective, our posterior estimate is significantly higher than the corresponding prior estimate for east Asia. The posterior estimate derived here is, however, consistent with results from recent studies focused on this region. We also find significant differences between the prior and posterior source estimates in other regions, notably south Asia, Indonesia, Europe, Central America/northern South America, and southern Africa. While qualitatively consistent with energy use trends in these regions, independent verification of the accuracy of our estimates is needed.

[44] In the context of future inverse-modeling studies aimed at characterizing sources of chemically important trace gases and aerosols, there is a pressing need to develop and apply more rigorous approaches for describing model and measurement error statistics. In particular, the effect of spatial error covariances on inferred source and error estimates must be investigated. In addition, possible biases in the measurements and models must be characterized and explicitly accounted for in the inverse approach. For characterizing model biases, a useful first step would be a rigorous inverse analysis intercomparison exercise using multiple CTMs to test the sensitivity of derived source estimates to differences in the underlying CTMs. On the longer term, comprehensive and integrated analysis approaches that make use of measurements of multiple chemical species from a variety of platforms are needed in order to fully exploit the potential of space-based tropospheric chemistry measurements to quantify the sources of chemically important trace gases and aerosols.

References

Allen, D., K. Pickering, and M. Fox-Rabinovitz (2004), Evaluation of pollutant outflow and CO sources during TRACE-P using model-calculated, aircraft-based, and Measurement of Pollution in the Troposphere (MOPITT)-derived CO concentrations, *J. Geophys. Res.*, 109, D15S03, doi:10.1029/2003JD004250.

Andreae, M. O. (1991), Biomass burning: Its history, use and distribution and its impact on environmental quality and global climate, in *Global Biomass Burning: Atmospheric, Climatic and Biospheric Implications*, edited by J. S. Levine, pp. 3–21, MIT Press, Cambridge, Mass.

Andreae, M. O., and P. Merlet (2001), Emission of trace gases and aerosols from biomass burning, *Global Biogeochem. Cycles*, 15, 955–966.

Arellano, A. F., P. S. Kasibhatla, L. Giglio, G. R. van der Werf, and J. T. Randerson (2004), Top-down estimates of global CO sources using MOPITT measurements, *Geophys. Res. Lett.*, 31, L01104, doi:10.1029/2003GL018609.

Bergamaschi, P., R. Hein, M. Heimann, and P. Crutzen (2000), Inverse modeling of the global CO cycle: 1. Inversion of CO mixing ratios, *J. Geophys. Res.*, 105, 1909–1927.

Bey, I., et al. (2001), Global modeling of tropospheric chemistry with assimilated meteorology: Model description and evaluation, *J. Geophys. Res.*, 106, 23,073–23,095.

Bousquet, P., P. Peylin, P. Ciais, M. Ramonet, and P. Monfray (1999), Optimization of annual atmospheric CO_2 net sources and sinks using inverse modeling: 2. Sensitivity study, *J. Geophys. Res.*, 104, 26,179–26,193.

Bousquet, P., et al. (2000), Regional changes in carbon dioxide fluxes of land and ocean since 1980, *Science*, 290, 1342–1346.

Bremer, H., et al. (2004), Spatial and temporal variation of MOPITT CO in Africa and South America: A comparison with SHADOZ ozone and MODIS aerosol, *J. Geophys. Res.*, 109, D12304, doi:10.1029/2003JD004234.

Butler, T. M., L. Simmonds, and P. J. Rayner (2004), Mass balance inverse modeling of methane in the 1990s using a chemistry transport model, *Atmos. Chem. Phys.*, 4, 2561–2580.

Carmichael, G. R., et al. (2003), Evaluating regional emission estimates using the TRACE-P observations, *J. Geophys. Res.*, 108(D21), 8810, doi:10.1029/2002JD003116.

Choi, Y., et al. (2005), Evidence of lightning NO_x and convective transport of pollutants in satellite observations over North America, *Geophys. Res. Lett.*, 32, L02805, doi:10.1029/2004GL021436.

Deeter, M. N., et al. (2003), Operational carbon monoxide retrieval algorithm and selected results for the MOPITT instrument, *J. Geophys. Res.*, 108(D14), 4399, doi:10.1029/2002JD003186.

Deeter, M. N., L. K. Emmons, D. P. Edwards, J. C. Gille, and J. R. Drummond (2004), Vertical resolution and information content of CO profiles retrieved by MOPITT, *Geophys. Res. Lett.*, 31, L15112, doi:10.1029/2004GL020235.

Dlugokencky, E., et al. (2001), Measurements of an anomalous global methane increase during 1998, *Geophys. Res. Lett.*, 28, 499–502.

Duncan, B. N., R. V. Martin, A. C. Staudt, R. Yevich, and J. A. Logan (2003), Interannual and seasonal variability of biomass burning emissions constrained by satellite observations, *J. Geophys. Res.*, 108(D2), 4100, doi:10.1029/2002JD002378.

Edwards, D. P., et al. (2003), Tropospheric ozone over the tropical Atlantic: A satellite perspective, *J. Geophys. Res.*, 108(D8), 4237, doi:10.1029/2002JD002927.

Edwards, D. P., et al. (2004), Observations of carbon monoxide and aerosols from the Terra satellite: Northern Hemisphere variability, *J. Geophys. Res.*, 109, D24202, doi:10.1029/2004JD004727.

Emmons, L. K., et al. (2004), Validation of Measurements of Pollution in the Troposphere (MOPITT) CO retrievals with aircraft in situ profiles, *J. Geophys. Res.*, 109, D03309, doi:10.1029/2003JD004101.

Fan, S., et al. (1998), A large terrestrial carbon sink in North America implied by atmospheric and oceanic carbon dioxide data and models, *Science*, 282, 442–446.

Fiore, A. M., et al. (2003), Variability in surface ozone background over the United States: Implication for air quality policy, *J. Geophys. Res.*, 108(D24), 4787, doi:10.1029/2003JD003855.

Gros, V., et al. (2004), Tracing the origin and ages of interlaced atmospheric pollution events over the tropical Atlantic Ocean with in situ measurements, satellites, trajectories, emission inventories, and global models, *J. Geophys. Res.*, 109, D22306, doi:10.1029/2004JD004846.

Guenther, A., et al. (1995), A global model of natural volatile organic compound emissions, *J. Geophys. Res.*, 100, 8873–8892.

Guenther, A., T. Karl, P. Harley, C. Wiedinmyer, P. Palmer, and C. Geron (2006), Estimates of global terrestrial isoprene emissions using MEGAN (Model of Emissions of Gases and Aerosols from Nature), *Atmos. Chem. Phys. Disc.*, 6, 107–173.

Gurney, K. R., et al. (2002), Towards robust regional estimates of CO_2 sources and sinks using atmospheric transport models, *Nature*, 415, 626–630.

Gurney, K. R., et al. (2003), Transcom 3 CO_2 inversion intercomparison: 1. Annual mean control results and sensitivity to transport and prior flux information, *Tellus, Ser. B*, 55(2), 555–579.

Gurney, K. R., et al. (2004), Transcom 3 inversion intercomparison: Model mean results for the estimation of seasonal carbon sources and sinks, *Global Biogeochem. Cycles*, 18, GB1010, doi:10.1029/2003GB002111.

Hatakeyama, S., et al. (1991), Reactions of OH with α-pinene and β-pinene in air: Estimate of global CO production from the atmospheric oxidation of terpenes, *J. Geophys. Res.*, 96, 947–958.

Heald, C. L., et al. (2003), Asian outflow and trans-Pacific transport of carbon monoxide and ozone pollution: An integrated satellite, aircraft, and model perspective, *J. Geophys. Res.*, 108(D24), 4804, doi:10.1029/2003JD003507.

Heald, C. L., et al. (2004), Comparative inverse analysis of satellite (MOPITT) and aircraft (TRACE-P) observations to estimate Asian sources of carbon monoxide, *J. Geophys. Res.*, 109, D23306, doi:10.1029/2004JD005185.

Hein, R., P. J. Crutzen, and M. Heimann (1997), An inverse modeling approach to investigate the global atmospheric methane cycle, *Global Biogeochem. Cycles*, 11, 43–76.

Houweling, S., T. Kaminski, F. Dentener, J. Lelieveld, and M. Heimann (1999), Inverse modeling of methane sources and sinks using the adjoint of a global transport model, *J. Geophys. Res.*, 104, 26,137–26,160.

Jacob, D., et al. (2002), Atmospheric budget of acetone, *J. Geophys. Res.*, 107(D10), 4100, doi:10.1029/2001JD000694.

Jacob, D., et al. (2003), The Transport and Chemical Evolution over the Pacific (TRACE-P) aircraft mission: Design, execution, and first results, *J. Geophys. Res.*, 108(D20), 9000, doi:10.1029/2002JD003276.

Jones, D. B., et al. (2003), Potential of observations from the Tropospheric Emission Spectrometer to constrain sources of carbon monoxide, *J. Geophys. Res.*, 108(D24), 4789, doi:10.1029/2003JD003702.

Kaminski, T., M. Heimann, and R. Giering (1999), A coarse grid three-dimensional global inverse model of the atmospheric transport: 2. Inversion of the transport of CO_2 in the 1980s, *J. Geophys. Res.*, 104, 18,555–18,581.

Kar, J., et al. (2004), Evidence of vertical transport of carbon monoxide from Measurements of Pollution in the Troposphere (MOPITT), *Geophys. Res. Lett.*, 31, L23105, doi:10.1029/2004GL021128.

Kasibhatla, P., A. F. Arellano, J. A. Logan, P. I. Palmer, and P. Novelli (2002), Top-down estimate of a large source of atmospheric carbon monoxide associated with fuel combustion in Asia, *Geophys. Res. Lett.*, 29(19), 1900, doi:10.1029/2002GL015581.

Lamarque, J. F., et al. (2003), Identification of CO plumes from MOPITT data: Application to the August 2000 Idaho-Montana forest fires, *Geophys. Res. Lett.*, 30(13), 1688, doi:10.1029/2003GL017503.

Langenfelds, R. L., et al. (2002), Interannual growth rate variations of atmospheric CO_2 and its $\delta^{13}C$, H_2, CH_4, and CO between 1992 and 1999 linked to biomass burning, *Global Biogeochem. Cycles*, 16(3), 1048, doi:10.1029/2001GB001466.

Law, R. M., and P. J. Rayner (1999), Impacts of seasonal covariance on CO_2 inversions, *Global Biogeochem. Cycles*, 13(4), 845–856.

Lelieveld, J., et al. (2004), Increasing ozone over the Atlantic Ocean, *Science*, 304, 1483–1487.

Li, Q., et al. (2005), North American pollution outflow and the trapping of convectively lifted pollution by upper-level anticyclone, *J. Geophys. Res.*, 110, D10301, doi:10.1029/2004JD005039.

Liu, J., J. R. Drummond, Q. Li, J. C. Gille, and D. C. Ziskin (2005), Satellite mapping of CO emission from forest fires in northwest America using MOPITT measurements, *Remote Sens. Environ.*, 95(4), 502–516.

Mikaloff Fletcher, S. E., P. P. Tans, L. M. Bruhwiler, J. B. Miller, and M. Heimann (2004a), CH_4 sources estimated from atmospheric observations of CH_4 and its $^{13}C/^{12}C$ isotopic ratios: 1. Inverse modeling of source processes, *Global Biogeochem. Cycles*, 18, GB4004, doi:10.1029/2004GB002223.

Mikaloff Fletcher, S. E., P. P. Tans, L. M. Bruhwiler, J. B. Miller, and M. Heimann (2004b), CH4 sources estimated from atmospheric observations of CH_4 and its $^{13}C/^{12}C$ isotopic ratios: 2. Inverse modeling of CH_4 fluxes from geographical regions, *Global Biogeochem. Cycles*, 18, GB4005, doi:10.1029/2004GB002224.

Müller, J.-F., and T. Stavrakou (2005), Inversion of CO and NO_x emission using the adjoint of the IMAGES model, *Atmos. Chem. Phys.*, 5, 1157–1186.

Olivier, J. G. J., et al. (1996), Description of EDGAR Version 2.0: A set of global emission inventories of greenhouse gases and ozone-depleting substances for all anthropogenic and most natural sources on a per country basis and on a $1° \times 1°$ grid, *Rep. 771060002*, Natl. Inst. of Public Health and the Environ., Bilthoven, Netherlands.

Palmer, P. I., et al. (2003), Inverting for emissions of carbon monoxide from Asia using aircraft observations over the western Pacific, *J. Geophys. Res.*, 108(D6), 4180, doi:10.1029/2002JD002153.

Pétron, G., et al. (2002), Inverse modeling of carbon monoxide surface emissions using CMDL network observations, *J. Geophys. Res.*, 107(D24), 4761, doi:10.1029/2001JD001305.

Pétron, G., et al. (2004), Monthly CO surface sources inventory based on the 2000–2001 MOPITT satellite data, *Geophys. Res. Lett.*, 31, L21107, doi:10.1029/2004GL020560.

Peylin, P., D. Baker, J. Sarmiento, P. Cias, and P. Bousquet (2002), Influence of transport uncertainty on annual mean and seasonal inversions of atmospheric CO_2 data, *J. Geophys. Res.*, 107(D19), 4385, doi:10.1029/2001JD000857.

Pfister, G., et al. (2004), Evaluation of CO simulations and the analysis of the CO budget for Europe, *J. Geophys. Res.*, 109, D19304, doi:10.1029/2004JD004691.

Prinn, R. G., et al. (2001), Evidence for substantial variation of atmospheric hydroxyl radicals in the past two decades, *Science*, 292, 1882–1888.

Rödenbeck, C., S. Houweling, M. Gloor, and M. Heimann (2003), Time-dependent atmospheric CO_2 inversions based on interannually varying tracer transport, *Tellus, Ser. B*, 55(2), 488–497.

Rodgers, C. (2000), *Inverse Methods for Atmospheric Sounding: Theory and Practice*, World Sci., Hackensack, N. J.

Shim, C., et al. (2005), Constraining global isoprene emissions with GOME formaldehyde column measurements, *J. Geophys. Res.*, 110, D24301, doi:10.1029/2004JD005629.

Suntharalingam, P. D., C. M. Spivakovsky, J. A. Logan, and M. B. McElroy (2003), Estimating the distribution of terrestrial CO_2 sources and sinks from atmospheric measurements: Sensitivity to configuration of the observation network, *J. Geophys. Res.*, 108(D15), 4452, doi:10.1029/2002JD002207.

Suntharalingam, P. D., et al. (2004), Improved quantification of Chinese carbon fluxes using CO_2/CO correlations in Asian outflow, *J. Geophys. Res.*, 109, D18S18, doi:10.1029/2003JD004362.

Tan, Q., et al. (2004), An evaluation of TRACE-P emission inventories from China using a regional model and chemical measurements, *J. Geophys. Res.*, 109, D22305, doi:10.1029/2004JD005071.

van der Werf, G. R., J. T. Randerson, G. J. Collatz, and L. Giglio (2003), Carbon emissions from fires in tropical and subtropical ecosystems, *Global Change Biol.*, 9, 547–562.

van der Werf, G. R., et al. (2004), Continental-scale partitioning of fire emissions during the 1997 to 2001 El Nino/La Nina period, *Science*, 303, 73–76.

Wang, Y., D. J. Jacob, and J. A. Logan (1998), Global simulation of tropospheric O_3-NO_x-hydrocarbon chemistry: 1. Formulation, *J. Geophys. Res.*, 103, 10,713–10,725.

Wang, Y. X., M. B. McElroy, T. Wang, and P. I. Palmer (2004), Asian emissions of CO and NO$_x$: Constraints from aircraft and Chinese station data, *J. Geophys. Res.*, *109*, D24304, doi:10.1029/2004JD005250.

————————————

A. F. Arellano Jr., Atmospheric Chemistry Division, National Center for Atmospheric Research, P. O. Box 3000, Boulder, CO 80307-3000, USA. (arellano@ucar.edu)

G. J. Collatz and L. Giglio, NASA Goddard Space Flight Center, Code 923, Greenbelt Road, Greenbelt, MD 20771, USA.

P. S. Kasibhatla, Nicholas School of the Environment and Earth Sciences, Duke University, Box 90328, Durham, NC 27708, USA.

J. T. Randerson, Department of Earth System Science, University of California, Irvine, 3212 Croul Hall, Irvine, CA 92697, USA.

G. R. van der Werf, Faculty of Earth and Life Sciences, Vrije Universiteit Amsterdam, De Boelelaan 1085, NL-1081 HV Amsterdam, Netherlands.